

Thickness-dependent thermal conductivity of ultrathin (< 100 nm) barium titanate films



Yechan Kim^a, Joonsuk Park^b, Jeongwoo Shin^c, Jihwan An^{c,*}, Jungwan Cho^{a,*}

^a Department of Mechanical Engineering, Kyung Hee University, 1732 Deogyong-daero, Giheung-gu, Yongin-si, Gyeonggi-do 17104, Republic of Korea

^b Department of Materials Science and Engineering, Stanford University, Stanford, CA 94305, United States

^c Department of Manufacturing Systems and Design Engineering, Seoul National University of Science and Technology, Seoul 139-743, Republic of Korea

ARTICLE INFO

Keywords:

High-dielectric-constant thin films
Barium titanate (BaTiO₃)
Thermal conductivity
Pulsed laser deposition (PLD)

ABSTRACT

Thin film barium titanate (BaTiO₃) is a promising material in the electronics and ceramics industry owing to its compelling dielectric properties. A number of works have investigated its dielectric and structural properties, but less studied are its thermal properties particularly at sub-100 nm thicknesses. Here, we measure the room-temperature thermal conductivity of ultrathin (< 100 nm), pulsed laser deposited BaTiO₃ films. The measured thermal conductivities are thickness-dependent, and this trend is consistent with the thickness-dependent crystallinity of the films. Transmission electron microscopy analysis of the films reveals the presence of an initial amorphous layer ~ 60 nm thick from the growth interface and the subsequent formation of columnar grains of width ~ 12 nm that are embedded within an amorphous matrix. For a region that incorporates grains with columnar morphology, we find that cross-plane heat conduction may be favored by 30–40% over in-plane heat conduction due to the columnar morphology of grains.

1. Introduction

Perovskite structured materials such as BaTiO₃ (BTO), SrTiO₃ (STO), or (Ba,Sr)TiO₃ (BST) have recently drawn lots of attention due to their compelling dielectric properties [1,2]. Perovskite thin films, for example, possess high dielectric constants (> 100) even at thicknesses less than 100 nm and are therefore attractive for applications such as dynamic random access memory (DRAM) capacitors or multilayer ceramic capacitors (MLCCs) [1–9]. Moreover, perovskite thin films have potential applications as thermoelectric materials for waste-energy harvesting or solid-state thermal management; their properties such as stability and non-toxicity and the controllability of carrier concentration by A and B cationic sites doping or oxygen vacancy control make them suitable for the thermoelectric applications [10,11]. With recent technological trends of electronic devices toward miniaturization, the use of such high-dielectric-constant perovskite thin films becomes even more indispensable, and therefore researches on the properties of perovskite thin films have recently been active.

While dielectric and structural properties of perovskite thin films have clearly been a key consideration in a number of previous works, there exist only a limited number of works that have investigated their thermal properties particularly at sub-100 nm thicknesses. One study [10] measured the room temperature thermal conductivities of

polycrystalline 170 nm STO films with average grain size ranging from 28 to 88 nm, which were reduced by approximately 50–60% as compared to that of bulk single crystal STO ($\sim 11 \text{ W m}^{-1} \text{ K}^{-1}$). Another study [11] observed a similar reduction in the room temperature thermal conductivity for thin film BTO samples compared with that of bulk single crystal BTO ($\sim 5.7 \text{ W m}^{-1} \text{ K}^{-1}$); the measured thermal conductivities of their polycrystalline 175 nm BTO films with average grain sizes of 36 and 63 nm were 1.0 and 1.7 $\text{W m}^{-1} \text{ K}^{-1}$, respectively. Given that the limiting dimension in these polycrystalline films is the grain size, these two previous studies suggest that the mean free paths of phonons that are important for carrying heat in complex oxide perovskites may be on the order of sub-100 nm [10,11]. More recently, we have reported the room temperature thermal conductivities of ~ 24 nm plasma-enhanced atomic layer deposited (PEALD) BTO films, which were partially crystalline within an amorphous matrix; the measured thermal conductivities of these films were approximately 0.9–1.1 $\text{W m}^{-1} \text{ K}^{-1}$ [12].

In this work, we report on the room-temperature thermal conductivity of BTO films with sub-100 nm thicknesses deposited by pulsed laser deposition (PLD) on Si substrates. We observe a dependence of the thermal conductivity on film thickness (0.59 ± 0.13 , 0.61 ± 0.07 , and $0.80 \pm 0.09 \text{ W m}^{-1} \text{ K}^{-1}$ for 30, 51, and 99 nm films, respectively), which is consistent with the film-thickness-dependent crystallinity.

* Corresponding authors.

E-mail addresses: jihwanan@seoultech.ac.kr (J. An), jungwan.cho@khu.ac.kr (J. Cho).

<https://doi.org/10.1016/j.ceramint.2018.09.228>

Received 10 July 2018; Received in revised form 10 September 2018; Accepted 19 September 2018

Available online 22 September 2018

0272-8842/ © 2018 Elsevier Ltd and Techna Group S.r.l. All rights reserved.

Transmission electron microscopy (TEM) analysis of the films suggest the presence of an initial amorphous layer up to approximately 60 nm from the growth interface and the subsequent formation of crystalline grains with columnar morphology that are embedded in an amorphous matrix. We further proceed to estimate local cross-plane and in-plane thermal conductivities for a region that contains columnar grains (i.e., located 60–99 nm away from the growth interface), and find values of approximately 1.1 and 0.7–0.8 W m⁻¹ K⁻¹, respectively. The columnar morphology of grains in this region is responsible for the anisotropic thermal conductivity, favoring cross-plane heat conduction by approximately 30–40% over in-plane heat conduction.

2. Material and methods

Three BTO films with different thicknesses were grown on p-doped Si substrates using PLD from a sintered BTO pellet (Kurt J. Lesker) as a target material. A Lambda Physik 248 nm KrF excimer laser was used. The laser intensity and frequency were 0.7 J/cm² and 10 Hz, respectively. The substrate temperature was kept at 500 °C, and the distance between the target and the substrate was 50 mm. The deposition was conducted in oxygen atmosphere at the pressure of 100 mTorr. The number of laser pulses were varied as 2000, 4000, and 8000 pulses, resulting in 30, 51, 99 nm-thick films, respectively, from the ellipsometry measurement.

The stoichiometry of the PLD BTO films is analyzed by X-ray photoelectron spectroscopy (XPS) in a SSI S-probe monochromatized XPS spectrometer with Al KR radiation (1486 eV). The crystalline phase and quality as well as the thicknesses of the PLD BTO films are analyzed by TEM (FEI 80–300 environmental (scanning) transmission electron microscope) at the acceleration voltage of 300 kV. Samples for the TEM analysis were prepared by using a focused ion beam (FEI Helios Dual-Beam Focused Ion Beam).

The cross-plane thermal conductivities of the three PLD BTO films are measured at room temperature with TDTR, an ultrafast, pump-probe, optical measurement technique [13–15]. For TDTR measurements, an ~49 nm Al film, which acts as an optothermal transducer layer, is deposited onto the surface of the BTO films by electron beam evaporation. Our setup [16,17] utilizes a mode-locked Nd:YVO₄ laser that emits 9.2 ps wide pulses at a repetition rate of 82 MHz and a wavelength of 1064 nm. These pulses are divided into two components: pump (heater) and probe (thermometer) beams. The frequency-doubled 532 nm, ~10.2 μm diameter pump beam, modulated at 6 MHz for lock-in detection, heats the topmost Al transducer layer. The time-delayed (up to 3.5 ns after the pump heating event) 1064 nm, ~6.2 μm diameter probe beam measures the temporal variations in the surface temperature of the Al transducer via proportional changes in the reflectivity of Al. At the pump beam modulation frequency, an RF lock-in amplifier records the in-phase (V_{in}) and out-of-phase (V_{out}) signals of the reflected probe beam as a function of pump-probe delay time. The amplitude ($\sqrt{V_{in}^2 + V_{out}^2}$) and/or ratio ($-V_{in}/V_{out}$) signals are compared

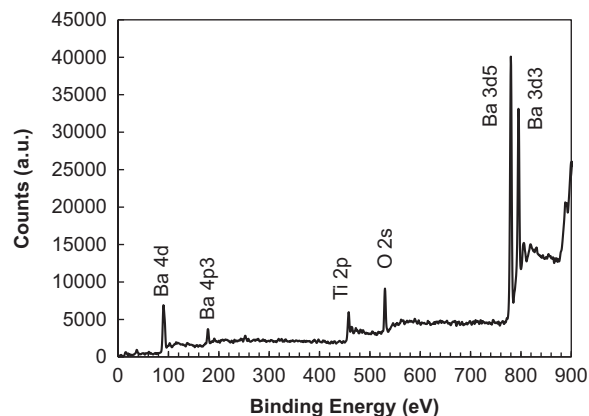


Fig. 2. XPS spectra of PLD BTO films.

to a multilayer heat diffusion model [13,14] to extract unknown thermal properties. For further descriptions of the TDTR methodology and corresponding data analysis, see Refs. [13–15].

3. Results and discussion

Fig. 1 shows cross-sectional TEM images of the PLD BTO samples. The TEM images of the 30 and 51 nm films indicate that these films are almost entirely amorphous. The TEM image of the thickest film reveals the presence of an initial amorphous layer about 60 nm thick from the growth interface and the subsequent formation of columnar crystalline grains of width ~12 nm, which are aligned normal to the growth interface and embedded in an amorphous matrix. XPS spectra in Fig. 2 shows the composition of PLD BTO films: Ba 20.3 at%, Ti 18.0 at%, and O 61.6 at%, which shows the Ba-to-Ti composition ratio of 1.13:1. The content of contaminations (e.g., carbon) are below the detection limit of the XPS analysis (< 0.1 at%).

The thermal properties of the samples are determined using TDTR by fitting the data to the multilayer heat diffusion model that has been discussed in detail elsewhere [13,14]. In our measurements, the temporal thermal response at the sample surface is related to the thicknesses, volumetric heat capacities and thermal conductivities of the Al transducer layer (d_{Al} , C_{Al} , k_{Al}), BTO layer (d_{BTO} , C_{BTO} , k_{BTO}), and Si Substrate (semi-infinite, C_{Si} , k_{Si}), along with the thermal boundary resistances at the Al/BTO and BTO/Si interfaces (TBR_{Al-BTO} , TBR_{BTO-Si}). For each sample, we determine d_{Al} and d_{BTO} from cross-sectional TEM images. The volumetric heat capacities of the Al layer and Si substrate (C_{Al} , C_{Si}) are taken from the literature [18,19]. The volumetric heat capacity of the BTO layer (C_{BTO}) is estimated from the product of the specific heat (~0.44 J g⁻¹ K⁻¹) taken from the literature [20] and the density (4.95 g cm⁻³) taken from our previous work for PEALD BTO films that were partially crystalline within an amorphous matrix [12].

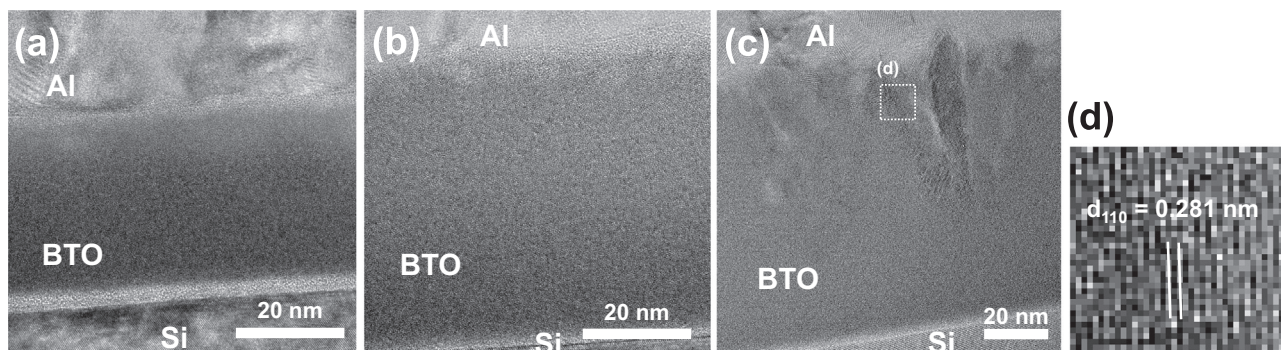


Fig. 1. Cross-sectional TEM images of PLD BTO thin films on Si: (a) 30 nm, (b) 51 nm, and (c) 99 nm films, and (d) a zoomed-in image of the white-dotted area in (c).

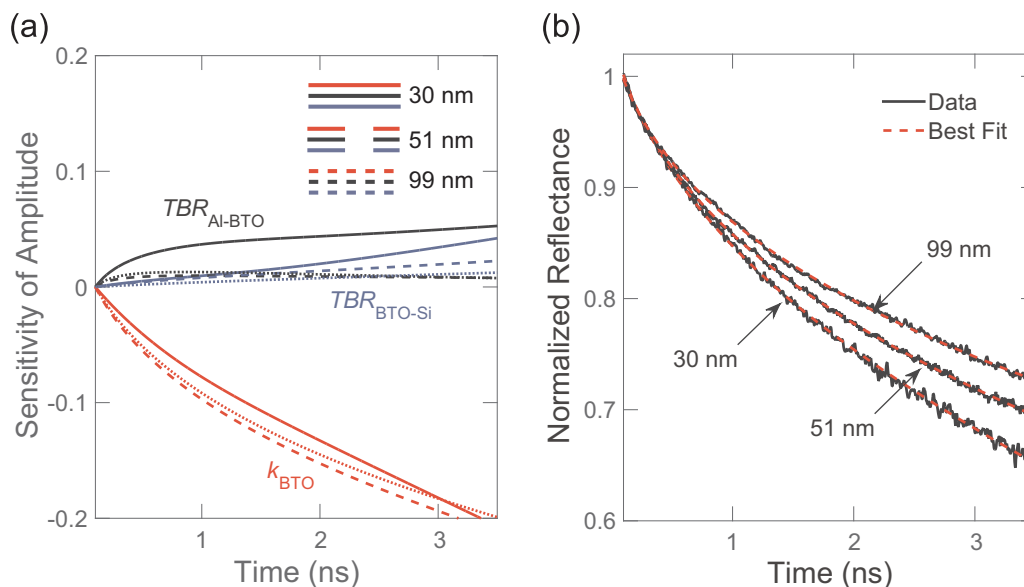


Fig. 3. (a) Sensitivities of TDTR amplitude ($\sqrt{V_{in}^2 + V_{out}^2}$) to the thermal conductivity of the BTO layer (red) and the thermal boundary resistances at the Al/BTO and BTO/Si interfaces (black and blue, respectively) for three BTO samples as a function of pump-probe time delay at 6-MHz pump modulation frequency. Solid, dashed, and dotted lines represent sensitivity curves for the 30 nm, 51 nm, and 99 nm samples, respectively. (b) TDTR amplitude data (black solid lines) and best-fit curves (red dashed lines) for the three BTO samples at 6-MHz pump modulation frequency. (For interpretation of the references to color in this figure legend, the reader is referred to the web version of this article.)

The density of amorphous BTO has been previously reported to be 4.3 g cm^{-3} [21]. Based on this difference in the BTO density, we assume an uncertainty of 13% in C_{BTO} , which propagates to uncertainties in k_{BTO} of 2%, 5%, and 7% for the 30, 51 and 99 nm samples, respectively. We calculate k_{Al} by measuring the in-plane electrical conductivity and using the Wiedemann-Franz law. We separately measure k_{Si} by TDTR on the Si substrate metallized with an $\sim 49 \text{ nm}$ Al film. We therefore have three unknowns in our thermal model: the thermal conductivity of the BTO layer (k_{BTO}) and the top side (Al/BTO) and bottom side (BTO/Si) thermal boundary resistances (TBR_{Al-BTO} , TBR_{BTO-Si}).

We quantify the measurement sensitivity to these three parameters by calculating $S_{\beta} = \partial \ln(R) / \partial \ln(\beta)$, where R is either the amplitude ($\sqrt{V_{in}^2 + V_{out}^2}$) or ratio ($-V_{in}/V_{out}$) signal and β is the parameter of interest [14–17,22]. As we discuss in detail below, we obtain k_{BTO} and TBR_{Al-BTO} by performing a two-parameter fit of the multilayer thermal model to the amplitude data, while treating TBR_{BTO-Si} as an input parameter determined from the ratio data.

Fig. 3(a) shows the sensitivities of the amplitude signal to these three unknown parameters for our BTO samples at 6 MHz pump modulation frequency. The sensitivity to k_{BTO} is relatively large and very dynamic over most of the delay time for all three samples, as compared to those to TBR_{Al-BTO} and TBR_{BTO-Si} , which implies that we are most sensitive to the thermal conductivity of the BTO layers (predominantly owing to their low thermal conductivity). The sensitivity to TBR_{Al-BTO} is much lower than that to k_{BTO} for all three samples; in particular, the measurements are almost insensitive to this top side boundary resistance for the 51 and 99 nm samples. But we allow TBR_{Al-BTO} to vary along with k_{BTO} to produce the best fit between the amplitude data and the thermal model. The sensitivity to TBR_{BTO-Si} is almost negligible for the 51 and 99 nm samples, while for the thinnest sample the sensitivity values of TBR_{BTO-Si} are comparable to those of TBR_{Al-BTO} (e.g., ~ 0.05 and ~ 0.04 for TBR_{Al-BTO} and TBR_{BTO-Si} , respectively, at a delay time of 3.5 ns). The sensitivity to in-plane heat conduction along the BTO layers is essentially zero for all three samples (although not shown for brevity in Fig. 3(a)), which implies that we are insensitive to the in-plane thermal conductivity of the BTO layers.

We analyze the ratio data for the thinnest sample, where the

volumetric resistance of the BTO layer is the lowest, at 6 MHz frequency and determine TBR_{BTO-Si} by utilizing higher sensitivity of the ratio to this bottom side boundary resistance than that of the amplitude [23,24]. In a similar procedure described previously [25], we consider an effective thermal conductivity that lumps the contributions from the top side interface and the BTO layer. We fit the ratio data to the thermal model with this effective thermal conductivity and the bottom side boundary resistance as two free parameters. This procedure yields the bottom side boundary resistance of $14.4 \pm 8.2 \text{ m}^2 \text{ K GW}^{-1}$, whose uncertainty is due to uncertainties in the thicknesses of the Al and BTO layers and the thermal properties of the Al layer and Si substrate. Our extracted TBR_{BTO-Si} value is consistent with the range reported in literature for high-dielectric-constant oxide/silicon interfaces [12,26–28]. Taking this value as the bottom side boundary resistance, we then fit the 6 MHz amplitude data to extract the thermal conductivity of the BTO layer and the top side boundary resistance. The reported uncertainty of $\sim 60\%$ in TBR_{BTO-Si} propagates to uncertainties in k_{BTO} of 17%, 7%, and 5% for the 30, 51, and 99 nm samples, respectively.

TDTR amplitude data and the corresponding best-fit thermal model at 6 MHz pump modulation frequency are shown in Fig. 3(b). We obtain the (cross-plane) BTO thermal conductivity to be $0.59 \pm 0.13 \text{ W m}^{-1} \text{ K}^{-1}$ for the 30 nm sample, $0.61 \pm 0.07 \text{ W m}^{-1} \text{ K}^{-1}$ for the 51 nm sample, and $0.80 \pm 0.09 \text{ W m}^{-1} \text{ K}^{-1}$ for the 99 nm sample. The errors reported on the best-fit values for the BTO thermal conductivity are calculated by propagating uncertainties in the Al thickness and thermal conductivity and the BTO thickness, as well as the BTO/Si thermal boundary resistance. The thermal boundary resistance at the Al/BTO interface is found to range from 6 to $13 \text{ m}^2 \text{ K GW}^{-1}$ for the three samples, which is consistent with values reported previously for metal-dielectric interfaces [15,17,29,30]. The variation observed between samples in this top side boundary resistance can be attributed to varying levels of impurities and contamination on the sample surface and of surface roughness [16,22,31,32].

We observe that the crystallinity of the PLD BTO films, which is thickness-dependent, impacts the measured thermal conductivities. The thermal conductivities of the 30 and 51 nm films are almost identical, in line with the observation made from the TEM images that both BTO films are almost entirely amorphous. The thermal conductivity of the

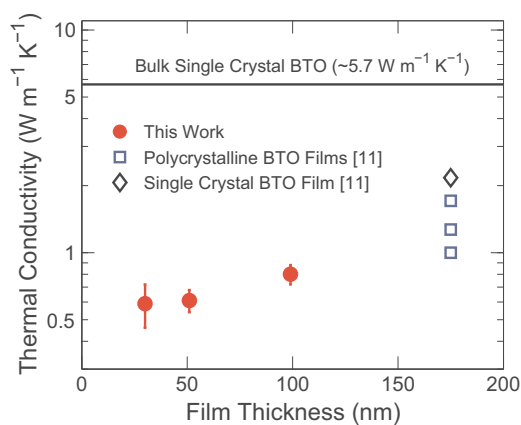


Fig. 4. Thermal conductivity of BTO films as a function of film thickness at room temperature. Filled circles represent the data for our PLD BTO films, open squares represent the data for polycrystalline, 175 nm BTO films with grain sizes of 36, 47, and 63 nm (lower, middle and upper ones, respectively) [11], and an open diamond represents the data for a single crystal, 175 nm BTO film [11]. The solid line at $k_{\text{BTO}} = 5.7 \text{ W m}^{-1} \text{ K}^{-1}$ denotes the thermal conductivity of bulk single crystal BTO [36].

thickest film is higher than those of the other two, thinner films, which is most likely due to increased heat conduction through the columnar crystalline grains of width $\sim 12 \text{ nm}$, located $\sim 60 \text{ nm}$ away from the growth interface and oriented parallel to the direction of heat flow, within this film. A number of studies have reported that grains with columnar morphology within a film helps improve cross-plane heat conduction [17,33–35].

Fig. 4 shows the room-temperature thermal conductivity of BTO films as a function of film thickness, including our PLD BTO data and the data by Donovan et al. [11], as well as the data for bulk single crystal BTO by Mante and Volger [36]. The data by Donovan et al. [11] are for polycrystalline, 175 nm BTO films, prepared by chemical solution deposition, with grain sizes of 36, 47, and 63 nm and a single crystal, 175 nm BTO film, epitaxially grown on a (001)-oriented single crystal STO substrate by RF magnetron sputtering. The thermal conductivities of our PLD BTO films are lower than those of four 175 nm BTO films [11] and bulk single crystal BTO [36]. This can be predominantly attributed to the amorphous nature of our PLD BTO films. Our thickest film contains columnar grains of width $\sim 12 \text{ nm}$, but they are located $\sim 60 \text{ nm}$ away from the growth interface and embedded within an amorphous matrix. It is well known that thermal conduction in amorphous materials is dictated by their disordered atomic structure and their thermal conductivity is therefore low as compared to their crystalline counterpart [37–39].

Given the thickness-dependent morphology of our PLD BTO films, we estimate the local cross-plane thermal conductivity within the BTO film, which depends on the distance (z) from the growth interface [40]. As discussed above, the film is almost entirely amorphous up to a thickness of about 60 nm and partially crystallized with columnar grains thereafter. Using the data for our different thickness samples (30, 51, and 99 nm), we determine the local cross-plane thermal conductivity corresponding to a region of $60 \text{ nm} < z < 99 \text{ nm}$. With the volumetric resistance of a region of $0 \text{ nm} < z < 60 \text{ nm}$ estimated from the data for the 30 and 51 nm films, we create a two-layer model within the 99 nm film: i.e., $\sim 49 \text{ nm}$ of Al on a 39 nm layer with unknown local cross-plane conductivity on a 60 nm layer with known properties on Si. We then fit for this local cross-plane conductivity and obtain a value of $\sim 1.1 \text{ W m}^{-1} \text{ K}^{-1}$. This fitted local conductivity is comparable to the conductivity values ($1.0\text{--}1.7 \text{ W m}^{-1} \text{ K}^{-1}$) of polycrystalline, 175 nm BTO films with grain sizes of 36–63 nm by Donovan et al. [11]. This is also comparable to the values ($0.9\text{--}1.1 \text{ W m}^{-1} \text{ K}^{-1}$) of $\sim 24 \text{ nm}$ PEALD BTO films, which were partially crystalline within an amorphous matrix, in

our previous work [12].

We make a further effort to estimate the local in-plane thermal conductivity, which is characteristic of a region of $60 \text{ nm} < z < 99 \text{ nm}$ within the film, and assess an anisotropy in thermal conductivity in this region of the film. Given the columnar morphology of grains that exist in this region, we employ a simple resistor model of crystalline and amorphous phases for both cross-plane and in-plane directions [34]. The crystalline and amorphous resistors act in parallel for the cross-plane direction and in series for the in-plane direction. Therefore, the local cross-plane and in-plane thermal conductivities (k_z and k_r , respectively) in this region can be modeled with the volume fraction of the crystalline phase (X_c) by

$$k_z = k_c X_c + k_a (1 - X_c), \quad (1)$$

$$\frac{1}{k_r} = \frac{X_c}{k_c} + \frac{1 - X_c}{k_a}, \quad (2)$$

where k_c and k_a are the thermal conductivities of crystalline and amorphous phases of BTO, respectively. Here, we assume $k_c = 2.17 \text{ W m}^{-1} \text{ K}^{-1}$ and $k_a = 0.6 \text{ W m}^{-1} \text{ K}^{-1}$. The latter is taken from the data for our 30 and 51 nm BTO films, both of which are almost entirely amorphous, while the former is taken from the data for a single crystal, 175 nm BTO film by Donovan et al. [11]. Utilizing the value of k_z obtained by our local cross-plane thermal conductivity fit, we estimate X_c to be ~ 0.3 from Eq. (1). Fixing this value, we then use Eq. (2) to estimate the local in-plane thermal conductivity and find $k_r = \sim 0.77 \text{ W m}^{-1} \text{ K}^{-1}$. This suggests that cross-plane heat conduction is favored over in-plane conduction in this region of the film with the anisotropy ratio ($\eta = k_r/k_z$) of ~ 0.7 . It is well known that the columnar morphology of grains gives rise to anisotropic thermal conductivity, with $k_r < k_z$ [17,24,33]. We note that the values of X_c and k_r estimated here depend on a specific choice of k_c . With assuming $k_c = 5.7 \text{ W m}^{-1} \text{ K}^{-1}$ from the data for bulk single crystal BTO [36], the estimated values of X_c and k_r become ~ 0.09 and $\sim 0.65 \text{ W m}^{-1} \text{ K}^{-1}$. This translates to $\eta = \sim 0.6$.

4. Conclusions

This work presents the experimental investigation of the thermal conductivity of PLD-grown BTO films of thickness 30, 51, and 99 nm using TDTR at room temperature. The measured thermal conductivities depend on film thickness (0.59 ± 0.13 , 0.61 ± 0.07 , and $0.80 \pm 0.09 \text{ W m}^{-1} \text{ K}^{-1}$ for 30, 51, and 99 nm films, respectively), which can be attributed to the film-thickness-dependent microstructure. The observations made in cross-sectional TEM images indicate the presence of an initial amorphous layer up to approximately 60 nm from the growth interface and the subsequent formation of crystalline grains with columnar morphology that are embedded in an amorphous matrix. For a region that incorporates columnar grains (i.e., located 60–99 nm away from the growth interface), heat conduction may be anisotropic, with local cross-plane and in-plane thermal conductivities estimated to be about 1.1 and $0.7\text{--}0.8 \text{ W m}^{-1} \text{ K}^{-1}$, respectively. The columnar morphology of grains in this region is responsible for anisotropic heat conduction, favoring cross-plane heat conduction by approximately 30–40% over in-plane heat conduction.

Acknowledgements

This work was supported by the National Research Foundation of Korea (NRF) grants funded by the Korea government (MSIT) (No. 2016R1C1B2015317, No. 2017M1A3A3A02016562 and No. 2018R1C1B6001150).

References

- [1] S.K. Kim, G.-J. Choi, S.Y. Lee, M. Seo, S.W. Lee, J.H. Han, H.-S. Ahn, S. Han,

- C.S. Hwang, Al-doped TiO₂ films with ultralow leakage currents for next generation DRAM capacitors, *Adv. Mater.* 20 (8) (2008) 1429–1435.
- [2] S.W. Lee, J.H. Han, S. Han, W. Lee, J.H. Jang, M. Seo, S.K. Kim, C. Dussarrat, J. Gatineau, Y.-S. Min, C.S. Hwang, Atomic layer deposition of SrTiO₃ thin films with highly enhanced growth rate for ultrahigh density capacitors, *Chem. Mater.* 23 (8) (2011) 2227–2236.
- [3] M. Vehkamäki, T. Hatanpää, T. Hänninen, M. Ritala, M. Leskelä, Growth of SrTiO₃ and BaTiO₃ thin films by atomic layer deposition, *Electrochem. Solid-State Lett.* 2 (10) (1999) 504–506.
- [4] S.W. Lee, O.S. Kwon, J.H. Han, C.S. Hwang, Enhanced electrical properties of SrTiO₃ thin films grown by atomic layer deposition at high temperature for dynamic random access memory applications, *Appl. Phys. Lett.* 92 (2008) 222903.
- [5] M. Vehkamäki, T. Hatanpää, M. Ritala, M. Leskelä, S. Väyrynen, E. Rauhala, Atomic layer deposition of BaTiO₃ thin films—Effect of barium hydroxide formation, *Chem. Vap. Depos.* 13 (5) (2007) 239–246.
- [6] R. Schafraneck, A. Giere, A.G. Balogh, T. Enz, Y. Zheng, P. Scheele, R. Jakoby, A. Klein, Influence of sputter deposition parameters on the properties of tunable barium strontium titanate thin films for microwave applications, *J. Eur. Ceram. Soc.* 29 (8) (2009) 1433–1442.
- [7] B. Chen, H. Yang, L. Zhao, J. Miao, B. Xu, X.G. Qiu, B.R. Zhao, X.Y. Qi, X.F. Duan, Thickness and dielectric constant of dead layer in Pt/(Ba_{0.7}Sr_{0.3})TiO₃/YBa₂Cu₃O_{7-x} capacitor, *Appl. Phys. Lett.* 84 (4) (2004) 583–585.
- [8] Y. Kim, P. Schindler, A.L. Dadlani, S. Acharya, J. Provine, J. An, F.B. Prinz, Plasma-enhanced atomic layer deposition of barium titanate with aluminum incorporation, *Acta Mater.* 117 (2016) 153–159.
- [9] P. Schindler, Y. Kim, D. Thian, J. An, F.B. Prinz, Plasma-enhanced atomic layer deposition of BaTiO₃, *Scr. Mater.* 111 (2016) 106–109.
- [10] B.M. Foley, H.J. Brown-Shaklee, J.C. Duda, R. Cheaito, B.J. Gibbons, D. Medlin, J.F. Ihlefeld, P.E. Hopkins, Thermal conductivity of nano-grained SrTiO₃ thin films, *Appl. Phys. Lett.* 101 (23) (2012) 231908.
- [11] B.F. Donovan, B.M. Foley, J.F. Ihlefeld, J.P. Maria, P.E. Hopkins, Spectral phonon scattering effects on the thermal conductivity of nano-grained barium titanate, *Appl. Phys. Lett.* 105 (8) (2014) 082907.
- [12] J. Cho, J. Park, F.B. Prinz, J. An, Thermal conductivity of ultrathin BaTiO₃ films grown by plasma-assisted atomic layer deposition, *Scr. Mater.* 154 (2018) 225–229.
- [13] D.G. Cahill, Analysis of heat flow in layered structures for time-domain thermoreflectance, *Rev. Sci. Instrum.* 75 (2004) 5119–5122.
- [14] A.J. Schmidt, X. Chen, G. Chen, Pulse accumulation, radial heat conduction, and anisotropic thermal conductivity in pump-probe transient thermoreflectance, *Rev. Sci. Instrum.* 79 (2008) 114902.
- [15] D.G. Cahill, P.V. Braun, G. Chen, D.R. Clarke, S. Fan, K.E. Goodson, P. Keblinski, W.P. King, G.D. Mahan, A. Majumdar, H.J. Maris, S.R. Phillpot, E. Pop, L. Shi, Nanoscale thermal transport. II. 2003–2012, *Appl. Phys. Rev.* 1 (2014) 011305.
- [16] J. Cho, Y. Li, W.E. Hoke, D.H. Altman, M. Asheghi, K.E. Goodson, Phonon scattering in strained transition layers for GaN heteroepitaxy, *Phys. Rev. B* 89 (2014) 115301.
- [17] A. Sood, J. Cho, K.D. Hobart, T.I. Feygelson, B.B. Pate, M. Asheghi, D.G. Cahill, K.E. Goodson, Anisotropic and inhomogeneous thermal conduction in suspended thin-film polycrystalline diamond, *J. Appl. Phys.* 119 (2016) 175103.
- [18] W.F. Giauque, P.F. Meads, The heat capacities and entropies of aluminum and copper from 15 to 300 K, *J. Am. Chem. Soc.* 63 (1941) 1897–1901.
- [19] P. Flubacher, A.J. Leadbetter, J.A. Morrison, Heat capacity of pure silicon and germanium and properties of their vibrational frequency spectra, *Philos. Mag.* 4 (1959) 273–294.
- [20] S.S. Todd, R.E. Lorenson, Heat capacities at low temperatures and entropies at 298.16 K. of metatitanates of barium and strontium, *J. Am. Chem. Soc.* 74 (8) (1952) 2043–2045.
- [21] J.C. Olson, D.F. Steverson, I. Bransky, The effect of temperature on properties of RF Sputtered BaTiO₃ films, *Ferroelectrics* 37 (1) (1981) 685–686.
- [22] J. Cho, D. Francis, D.H. Altman, M. Asheghi, K.E. Goodson, Phonon conduction in GaN-diamond composite substrates, *J. Appl. Phys.* 121 (5) (2017) 055105.
- [23] J. Cho, J. Park, J. An, Low thermal conductivity of atomic layer deposition yttria-stabilized zirconia (YSZ) thin films for thermal insulation applications, *J. Eur. Ceram. Soc.* 37 (9) (2017) 3131–3136.
- [24] J. Cho, Thermal properties of anisotropic and/or inhomogeneous suspended thin films assessed via dual-side time-domain thermoreflectance: a numerical study, *Nanoscale Microsc. Thermophys. Eng.* 22 (1) (2018) 6–20.
- [25] A. Giri, J.P. Niemelä, C.J. Szwejkowski, M. Karppinen, P.E. Hopkins, Reduction in thermal conductivity and tunable heat capacity of inorganic/organic hybrid superlattices, *Phys. Rev. B* 93 (2) (2016) 024201.
- [26] M.A. Panzer, M. Shandalov, J.A. Rowlette, Y. Oshima, Y.W. Chen, P.C. McIntyre, K.E. Goodson, Thermal properties of ultrathin hafnium oxide gate dielectric films, *IEEE Electron Device Lett.* 30 (12) (2009) 1269–1271.
- [27] J.T. Gaskins, P.E. Hopkins, D.R. Merrill, S.R. Bauers, E. Hadland, D.C. Johnson, D. Koh, J.H. Yum, S. Banerjee, B.J. Nordell, M.M. Paquette, A.N. Caruso, W.A. Lanford, P. Henry, L. Ross, H. Li, L. Li, M. French, A.M. Rudolph, S.W. King, Investigation and review of the thermal, mechanical, electrical, optical, and structural properties of atomic layer deposited high-k dielectrics: beryllium oxide, aluminum oxide, hafnium oxide, and aluminum nitride, *ECS J. Sol. State Sci. Technol.* 6 (10) (2017) N189–N208.
- [28] E.A. Scott, J.T. Gaskins, S.W. King, P.E. Hopkins, Thermal conductivity and thermal boundary resistance of atomic layer deposited high-k dielectric aluminum oxide, hafnium oxide, and titanium oxide thin films on silicon, *APL Mater.* 6 (5) (2018) 058302.
- [29] R.J. Stevens, A.N. Smith, P.M. Norris, Measurement of thermal boundary conductance of a series of metal-dielectric interfaces by the transient thermoreflectance technique, *J. Heat Transf.* 127 (3) (2005) 315–322.
- [30] H.K. Lyeo, D.G. Cahill, Thermal conductance of interfaces between highly dissimilar materials, *Phys. Rev. B* 73 (14) (2006) 144301.
- [31] P.E. Hopkins, L.M. Phinney, J.R. Serrano, T.E. Beechem, Effects of surface roughness and oxide layer on the thermal boundary conductance at aluminum/silicon interfaces, *Phys. Rev. B* 82 (2010) 085307.
- [32] C.S. Gorham, K. Hattar, R. Cheaito, J.C. Duda, J.T. Gaskins, T.E. Beechem, J.F. Ihlefeld, L.B. Biedermann, E.S. Piekos, D.L. Medlin, P.E. Hopkins, Ion irradiation of the native oxide/silicon surface increases the thermal boundary conductance across aluminum/silicon interfaces, *Phys. Rev. B* 90 (2014) 024301.
- [33] J.E. Graebner, S. Jin, G.W. Kammlott, J.A. Herb, C.F. Gardinier, Large anisotropic thermal conductivity in synthetic diamond films, *Nature* 359 (6394) (1992) 401.
- [34] J. Lee, Z. Li, J.P. Reifenberg, S. Lee, R. Sinclair, M. Asheghi, K.E. Goodson, Thermal conductivity anisotropy and grain structure in Ge₂Sb₂Te₅ films, *J. Appl. Phys.* 109 (2011) 084902.
- [35] B.T. Kearney, B. Jugdersuren, D.R. Queen, T.H. Metcalf, J.C. Culbertson, P.A. Desario, X. Liu, et al., From amorphous to nanocrystalline: the effect of nanograins in an amorphous matrix on the thermal conductivity of hot-wire chemical-vapor deposited silicon films, *J. Phys.: Condens. Matter* 30 (8) (2018) 085301.
- [36] A.J.H. Mante, J. Volger, The thermal conductivity of BaTiO₃ in the neighbourhood of its ferroelectric transition temperatures, *Phys. Lett. A* 24 (3) (1967) 139–140.
- [37] D.G. Cahill, S.K. Watson, R.O. Pohl, Lower limit to the thermal conductivity of disordered crystals, *Phys. Rev. B* 46 (1992) 6131–6140.
- [38] J.L. Feldman, M.D. Kluge, P.B. Allen, F. Wooten, Thermal conductivity and localization in glasses: numerical study of a model of amorphous silicon, *Phys. Rev. B* 48 (17) (1993) 12589.
- [39] J.L. Braun, C.H. Baker, A. Giri, M. Elahi, K. Artyushkova, T.E. Beechem, P.M. Norris, Z.C. Leseman, J.T. Gaskins, P.E. Hopkins, Size effects on the thermal conductivity of amorphous silicon thin films, *Phys. Rev. B* 93 (14) (2016) 140201.
- [40] J. Cho, D. Francis, P.C. Chao, M. Asheghi, K.E. Goodson, Cross-plane phonon conduction in polycrystalline silicon films, *J. Heat Transf.* 137 (7) (2015) 071303.